Why electrochromism in $Li_4Ti_5O_{12}$ differs in the visible and infrared spectrum†

Meng Li[a,b], Tim Gould*[b], Zhong Su[a] and Shanqing Zhang*[a]

$Li_4Ti_5O_{12}$ (LTO) has been experimentally proven as a promising electrochromic material in applications of smart windows, thermal management and infrared camouflage. However, the fundamental mechanism on these phenomena is still lacking. For the first time, we fill this knowledge gap via quantitative matching the LTO's optical properties and electronic structure during charging/discharging using density functional theory. Our study suggests that the absorption of infrared is highly sensitive to intercalation of Li in the LTO lattice, in contrast with the adsorption of visible wavelengths. This unique property of LTO offers the practical ability in controlling infrared-induced heating with minimal effect on transmission of visible light. Furthermore, we also conclude that electrochemically controlled intercalation of Li causes donor states to appear, expand and move to deeper levels in the forbidden band, leading to better conductivity and lower transmittance, which is in line with the experimental results in the literature.

Electrochromism is a phenomenon related to the reversible changes in optical properties (*e.g.* absorbance, transmittance, reflectance) of a material induced by externally applied potentials. Interest in visible electrochromism has been wide-ranging, from inorganic compounds (*e.g.* Prussian blue analogs and WO_3 to organic polymers (*e.g.* polyaniline). Commercial electrochromic applications have become more widespread and extensive in recent years, from auto-dimming rearview mirrors to smart windows. The latter is a major application area due to the popularity of large window panes in non-residential buildings. Smart glass can meet the design aspirations of increasing glazing and reducing the use of electric lighting, which makes them very attractive, especially in view of global warming.

Typically, understanding and application of electrochromism focuses on the visible spectrum. However, electrochromism also occurs in the infrared region, which has been largely ignored before. There are, at present, two easily-identified practical applications for infrared electrochromics: infrared camouflage and thermal management. The first application can help vehicles and persons blend into the environment and consequently become invisible to infrared detection devices through reducing infrared emittances. The second application is using electrochromic devices to control temperature by tuning the infrared radiative heating on the illuminated object, which can reduce electricity consumption and thus the dependence on the cooling and heating system. As infrared (above 700 nm) accounts for 52 to 55 percent of the energy of sunlight at Earth's surface, taking full advantage of the energy in this spectrum can produce huge social and economic benefits. After decades of years of active research in the field of electrochromism, there are still significant challenges to be met. These include large tunability, excellent durability, reduced switching times and low manufacturing costs.

Recently, Mandal *et al.*[1] reported the visible-to-infrared broadband electrochromic properties of $Li_4Ti_5O_{12}$ (LTO), which is a promising anode material because of its notable "zero-strain" characteristic. During the lithium intercalation-deintercalation process, LTO has negligible structural change and can maintain excellent electrochemical performance over a large number of cycles with a stable voltage plateau of 1.5 V versus Li^+/Li, which help prevent the formation of metallic Li dendrites. More importantly, LTO has a highly contrasting optical behavior between uncharged state ($Li_4Ti_5O_{12}$) and charged state ($Li_7Ti_5O_{12}$), together with superior thermal stability. The above advantages make LTO a promising electrochromic material. However, understanding of the mechanisms responsible for the LTO electrochromism is still lacking. For example, researchers[1] believe that $Li_4Ti_5O_{12}$ has a high reflectance when nanostructured, compared to $Li_7Ti_5O_{12}$. Firstly, this explanation violates the general rule that the better the conductivity, the higher the reflectivity. Secondly, this high reflectivity is mainly contributed by the substrate material (Al), which is coated by a low absorbance material ($Li_4Ti_5O_{12}$). Due to the limitations of objective conditions in experiments, for example, measurements of reflection and absorp-

[a] *Centre for Clean Environmental and Energy and School of Environment and Science, Gold Coast Campus, Griffith University, QLD 4222, Australia. Fax: +61 5552 8067; Tel: +61 5552 8155; E-mail: s.zhang@griffith.edu.au*

[b] *Queensland Micro- and Nanotechnology Centre, Nathan Campus, Griffith University, QLD 4111, Australia. E-mail: t.gould@griffith.edu.au*

† Electronic Supplementary Information (ESI) available: [details of any supplementary information available should be included here]. See DOI: 10.1039/cXCP00000x/

tion coefficients may interfere with each other because of their simultaneous occurrence, theoretical research is urgently needed to supplement this.

To the best of our knowledge, some basic properties of LTO are still unknown: (i) detailed optical properties have not been calculated, particularly in the infrared region; (ii) the corresponding electronic structure of LTO have not been quantitatively investigated during charging/discharging process, and the bonding mechanism has not been clearly understood; (iii) the electronic structure-property relationship has not been discussed or analyzed. Namely, the underlying mechanism of its electrochromism has not been made clear. Therefore, to fill these gaps, the structural, electronic, and optical properties of LTO are studied by density functional theory (DFT) in the present work (specifically, PBE+U and HSE06 - details later). Our results thus help interpret and refine previous experimental conclusions, and offer insights into future work.

1 Calculation Method

The crystal structure of spinel $Li_4Ti_5O_{12}$ belongs to the $Fd\bar{3}m$ space group (No. 227). Li and O ions occupy the tetrahedral 8*a* sites and the octahedral 32*e* sites, respectively, while 1/6 of the octahedral 16*d* sites are randomly occupied by Li and Ti located at the remaining 5/6 of 16*d* sites. The structure can be described as $[Li_3]_{8a}[LiTi_5]_{16d}[O_{12}]_{32e}$. In order to satisfy the stoichiometry of $Li_4Ti_5O_{12}$, a $1\times1\times3$ supercell model is constructed to give the appropriate ratio of all elements. In theory, there are many different structures, and so we adopt the a structure found in the literature,[2] which has the lowest total energy per unit cell. Our model is built by considering that the charging process of $Li_4Ti_5O_{12}$ to $Li_7Ti_5O_{12}$ has been proved to be is a two-phase process, so our structures for $Li_{4+x}Ti_5O_{12}$ (x=0.125, 1, 2, 3) have the Li concentrated locally to conform with experiments.

Spin-polarized DFT calculations[3,4] were performed as implemented in the Vienna *ab initio* Simulation Package (VASP),[5,6] using generalized gradient approximation (GGA) parameterized by Perdew-Burke-Ernzerhof (PBE).[7] The interaction potentials of the core electrons were replaced by projector augmented wave (PAW)[8] pseudopotentials (Li_sv, Ti_pv, O). As Ti-3d states have strong on-site Coulomb interaction of localized electrons, which are not correctly described by LDA or GGA, DFT+U corrections were introduced with U = 2.5 eV.[9,10] The cutoff energy for the plane-wave basis was 600 eV for all calculations.

For structure relaxation, the k-point meshes for Brillouin zone sampling were $3\times3\times1$ Γ centered Monkhorst-Pack grids, with a small broadening width of Gaussian smearing (0.05 eV). The energy difference and force required for convergence were set to 10^{-6} eV and 0.01 eV/Å, respectively, which achieved a reasonable balance between accuracy and numerical cost. All atoms were fully relaxed to simulate the optimized structure of each lattice model.

For optical properties calculation, the number of bands were tripled, compared to the ground state (*i.e.,* we used twice the number of unoccupied bands as occupied). To better understand the band gap of LTO, we also carried out Heyd-Scuseria-Ernzerhof (HSE06) hybrid functional calculations of the density of states (DOS),[11–14] with the k-space sampled only by the Γ point. HSE06 is generally better at predicting energy gaps, but is significantly more costly than PBE+U, which meant we could not use it for all applications. Results from PBE+U were in generally good agreement with HSE06, supporting its use for other calculations. Details are provided in the Electronic Supplementary Information (ESI).

2 Optical properties

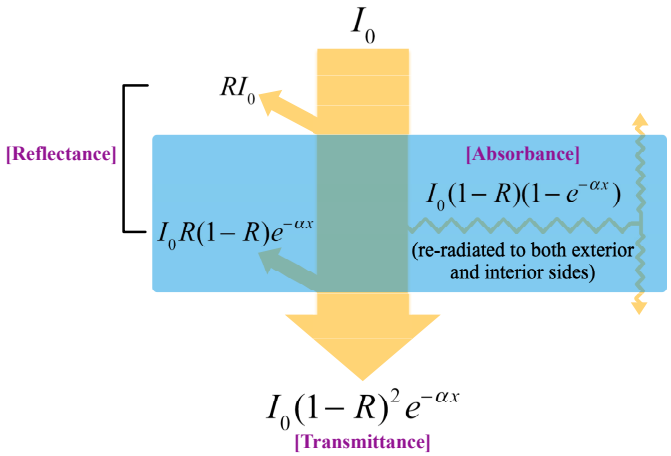

Fig. 1 The schematic diagram of energy loss of vertical light radiation through LTO material. Secondary and multiple reflections from the interface (LTO/air) within the LTO material are not depicted.

Experimental results are usually for transmission of light. However, calculations typically reveal the reflectance and adsorption. Therefore we need to relate these quantities.

Let us begin by summarizing some basic properties of how light and materials interact. The light radiation falling onto a material will be reflected, absorbed and transmitted, depending upon the wavelength (λ) of the radiation, the incident angle and material thickness, as well as the optical properties of the material, which includes reflectivity, absorption, scattering coefficient and surface finish. A schematic diagram is shown in Figure 1, for the case of negligible scattering. The material's transmittance (T), absorbance (A) and reflectance (R) are then subject to the equation:[15]

$$T(\lambda)+A(\lambda)+R(\lambda)=I_0$$

According to the Beer-Lambert law (α: absorption; x: thickness):

$$A(\lambda)=I_0(1-e^{-\alpha x})$$

adsorption is zero at the upper surface (x=0) of a material. Here, the vertical incident light intensity is I_0, and the upper surface reflection loss is RI_0, meaning that the light intensity entering into LTO is $I_0(1-R)$. Passing through LTO with a thickness of x causes energy loss, which equals $I_0(1-R)(1-e^{-\alpha x})$, due to absorption. When reaching the lower surface, the light intensity is only $I_0(1-R)e^{-\alpha x}$, and part of the light ($I_0R(1-R)e^{-\alpha x}$) will be reflected into the interior of the material, and the light intensity actually passing through LTO is $I_0(1-R)^2e^{-\alpha x}$. Next, the electrochromic properties of LTO materials in different wavelength ranges will be

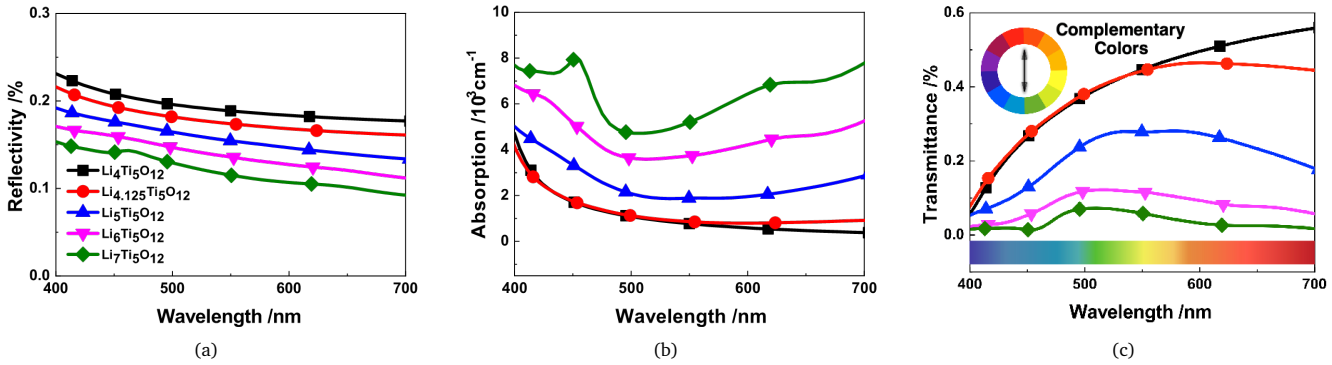

Fig. 2 (a) and (c) depict % reflectivity and transmittance, respectively. (b) shows the absorption spectrum of LTO material in cm^{-1}

discussed in detail.

2.1 Under visible spectrum (VIS, 400-700 nm)

Visible light falls between the infrared (with longer wavelengths) and the ultraviolet (with shorter wavelengths) in the electromagnetic spectrum, with wavelengths in the range of 400-700 nm.[16,17]

For $Li_4Ti_5O_{12}$ (black curve in Figure 2), the reflection coefficients of different wavelengths are almost the same, but the absorption coefficient decreases rapidly in the range of 400-500 nm, followed by slow decline after 500 nm. Therefore, taking a 5 μm thick LTO as an example, the corresponding transmittance curve of $Li_4Ti_5O_{12}$ increases rapidly in the wavelength of 400-500 nm, and this high transmittance has a slow growth in the range of 500-700 nm. For the charged state $Li_7Ti_5O_{12}$ (green curve in Figure 2), the reflectance coefficient for different wavelengths of light is reduced by the maximum of about 10%. However, the increase of absorption coefficient in the visible band is extremely large, with the minimal value at around 500 nm. As a result, transmittance reaches the maximum value in the same wavelength, which is different from the range in the literature (400-500 nm).[18] This is likely to be the result of red shift caused by the PBE method, which is known to underestimate band gaps.

The reflection, absorption, and transmission properties of intermediate transition states are between those of $Li_4Ti_5O_{12}$ and $Li_7Ti_5O_{12}$. In general, the change in reflectivity is negligible, and the change in the absorption coefficient dominates in optical properties. This theoretical result is in good agreement with reported experimental transmittance.[18] The reason why the glass containing LTO (as reported in Ref. 18) changed from transparent to black in the experiment can be explained by calculating the transmittance (T) under sunlight (λ_1=400 nm, λ_2=700 nm):

$$T = \frac{\sum_{\lambda_1}^{\lambda_2} T(\lambda) S_\lambda \Delta\lambda}{\sum_{\lambda_1}^{\lambda_2} S_\lambda \Delta\lambda} \quad (1)$$

where S_λ is relative spectral distribution of solar radiation, T(λ) is spectral transmittance of LTO and λ is wavelength. If the thickness of LTO is 5 μm, $Li_4Ti_5O_{12}$ has a transmittance of 41.7%, which means that nearly half of the total energy of visible light can go through this material. By contrast, the value for $Li_7Ti_5O_{12}$ is only 3.8%, which makes it impossible for visible light to transfer through LTO and makes LTO appear black. Considering that secondary and multiple reflections from the interface (LTO/air) within the LTO material can increase transmittance, especially for the material with low absorption coefficient ($Li_4Ti_5O_{12}$), the range of adjustable light transmittance is likely to be larger than calculated. To put these results in context, commercially available oxide-based electrochromic glasses are generally designed with a double electrochromic (active) layer, and the most popular design is WO_3 cooperated with $Ni(OH)_2$. The maximum visible transmittance that can be found ranges from 1% to 60%.[19] Considering that a single active layer of LTO can achieve a transmittance of 3.8%-41.7%, the electrochromic properties of LTO are excellent, and close to the performance of commercial products with dual active layers.

Another experimental phenomenon reported in the literature[21] is that LTO turns blue before it turns black. This is because after embedding with a small amount of Li, for example to form $Li_{4.125}Ti_5O_{12}$, LTO absorbs more light in the wavelength of 600-700 nm, corresponding to red-orange color. According to Figure 2(c) and the solar spectrum at the Earth's surface, the transmitted energy of sunlight of different color through a 5 μm thick LTO can be obtained through integration, which is listed in Table 1. Considering the existence of the redshift, the red and orange light will be absorbed more in $Li_{4.125}Ti_5O_{12}$ ($T_{charged}$), compared to $Li_4Ti_5O_{12}$ ($T_{uncharged}$). Therefore, LTO shows the corresponding complementary color (the color wheel in Figure 2(c)), a mixture of blue and green.

2.2 Under infrared spectrum (IR, 0.7-15 μm)

Under the same wavelength of solar spectrum, both the reflectivity and absorption coefficient of LTO (Figure 3(a)&3(b)) are increased in general during lithiation, although the reflectivity coefficient is slightly reduced in the wavelength of 0.25-1.5 μm. Compared to mild rising of reflectivity coefficient, the absorption coefficient has increased by four orders of magnitude, which helps $Li_4Ti_5O_{12}$ change from an infrared transmission material to an infrared absorption material.

The calculated transmittance of a 5 μm thick LTO is shown in Figure 3(c) as an example. It shows that $Li_4Ti_5O_{12}$ is transparent to visible light and infrared, while for $Li_7Ti_5O_{12}$, a consider-

Table 1 Transmitted energy of sunlight of different color

Color	Wavelength /nm	$T_{uncharged}$ /W· m^2	$T_{charged}$ /W· m^2	$T_{charged}/T_{uncharged}$
Violet	380-450	8.973	9.683	108%
Blue	450-495	18.96	19.24	101%
Green	495-570	42.65	42.62	100%
Yellow	570-590	12.75	12.29	96%
Orange	590-620	19.73	18.34	93%
Red	620-750	84.47	69.27	82%

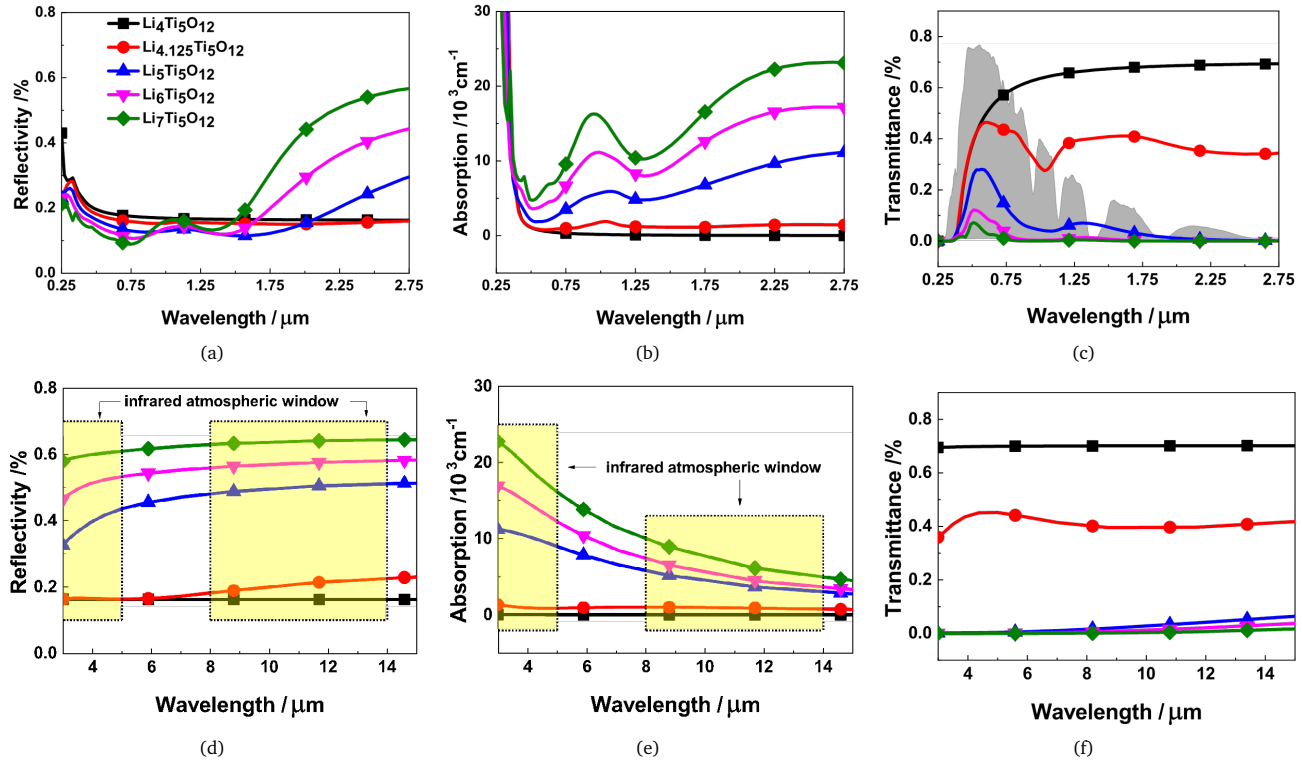

Fig. 3 (a), (b) and (c) are the reflectivity, absorption and transmittance spectrum, and the grey area is the AM 1.5 solar spectrum. (d), (e) and (f) are the reflectivity, absorption and transmittance spectrum under mid-wavelength infrared (MWIR, 3-8 μm) and long-wavelength infrared (LWIR, 8-15 μm).[20]

able part of visible light is absorbed as well as almost all infrared in the wavelength of the solar spectrum. More importantly, the transmittance of $Li_{4.125}Ti_5O_{12}$, which is intercalated with a small amount of Li in $Li_4Ti_5O_{12}$, has a rapid decrease in the infrared range.

Quantitative results are shown in Figure 4, using Equation 1 in the range of infrared (IR), visible light (VIS) and ultraviolet (UV). For $Li_4Ti_5O_{12}$, the transmitted energy of IR and VIS accounts for 35%, 17% of the total energy of sunlight, respectively. After charging to $Li_{4.125}Ti_5O_{12}$, the energy of transmitted VIS decreases to 16%, while transmitted IR shows a more substantial drop from 35% to 21% . When charged to $Li_5Ti_5O_{12}$, transmitted VIS decreases by 47% (from 17% to 9%) compared to the uncharged state, and transmitted IR is reduced by nearly 90% (from 35% to 4%). This means a small amount of intercalated Li in LTO can greatly reduce transmittance of IR while maintaining transmittance of VIS. As infrared has a significant thermal effect, LTO can help prevent the infrared radiation on one side from warming up.

In the infrared range with longer wavelength (3-15 μm), both reflection and absorption coefficients increase as x increases in $Li_{4+x}Ti_5O_{12}$ $(0 \leq x \leq 3)$. There are two important infrared atmosphere windows, 3-5 μm and 8-14 μm, which are the operating wavelength ranges of infrared detection equipment and are signed in light yellow in Figure 3(d)&3(e). The transmittance curve in Figure 3(f) shows good adjustable performance in these two windows, from 70% to nearly 0% as x increases in $Li_{4+x}Ti_5O_{12}$. This means LTO can "appear" or "disappear" in infrared detection equipment by applied voltage.[22]

3 Electronic structure

3.1 DOS graph and the molecular-orbital bonding diagram

After reporting the results revealed by our study, we now turn to explaining them. The highly contrasting optical behavior of $Li_4Ti_5O_{12}$ and $Li_7Ti_5O_{12}$ can be attributed to their respective electronic structures. Figure 5 reports density of states (DOS) and partial DOS results. $Li_4Ti_5O_{12}$ is a semiconductor with a calculated band gap of about 3.93 eV, slightly larger than results (3.87 eV, 3.73 eV) in the literature.[23,24]

The charging process from $Li_4Ti_5O_{12}$ to $Li_7Ti_5O_{12}$ involves Li

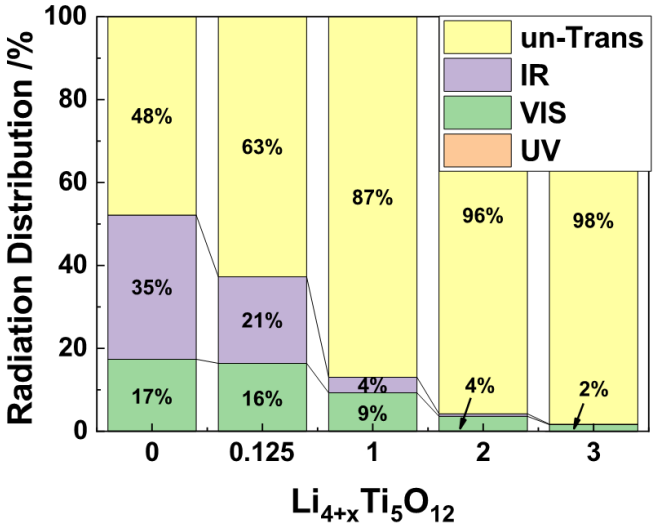

Fig. 4 The distribution of transmitted energy under sunlight (VIS: visible light, 0.4-0.7 μm; IR: infrared, 0.7-2.75 μm; 100% equals to the total energy of the AM 1.5 solar spectrum.). Ultraviolet (UV, 0.01-0.4 μm) contributions are essentially zero (maximum 0.06%) in all cases.

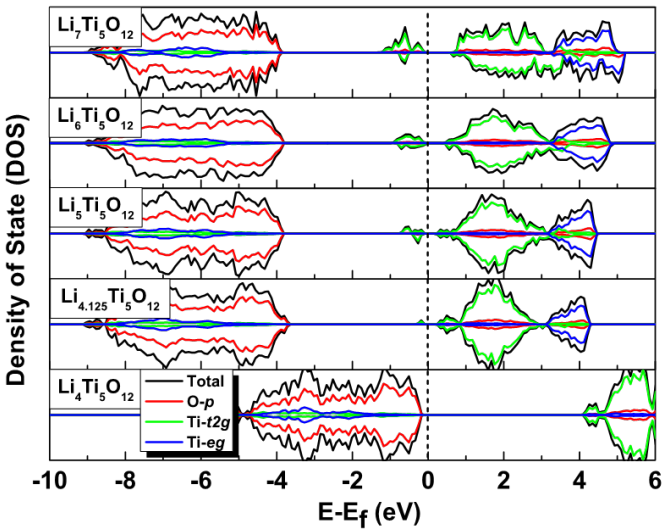

Fig. 5 Total and projected densities of states (DOS). The Fermi level is aligned to zero.

doping into LTO. A Li atom can easily lose an electron, forming a positive electric center and a redundant electron. As the electronegativity of Ti (1.54) is larger than Li (0.98), this excess electron is more likely to be captured by Ti and occupy the d_{xy} orbit, which lifts the Fermi level and forms donor states next to the conduction band (CB), revealed by the peak on the left side of the Fermi level in Figure 5. In fact, the electrons in the d_{xy} orbit are weakly bounded by Ti, and can easily overcome the donor ionization energy with only a small amount of energy, entering into the CB to be free electrons. This kind of impurity excitation is much easier than intrinsic excitation, which excites electrons in the valence band (VB) to the CB directly. That's why the conductivity can be greatly improved by the donor states. According to Maxwell's equations, the relationship between conductivity (σ) and absorption coefficient (α) can be expressed as:

$$\alpha^2 = 2\mu\mu_0\varepsilon\varepsilon_0\omega^2\left\{\left[1+\left(\frac{\sigma}{\mu\varepsilon\varepsilon_0\omega}\right)^2\right]^{\frac{1}{2}}-1\right\}$$

Where ε is the permittivity and μ the permeability of the material; ε_0 is the permittivity of free space and μ_0 the permeability of free space; ω is angular frequency. For a poorly conductive material ($\omega \to 0$), the absorption coefficient (α) is easily shown to be nearly zero from the equation above. However, for a good conductive material, the absorption coefficient (α) can be very large:

$$\alpha \approx \sqrt{2\mu_0\omega\sigma} \qquad \left[\text{when } \frac{\sigma}{\mu\varepsilon\varepsilon_0\omega} \gg 1\right]$$

As a result, due to the appearance of the donor states, the conductivity is improved, which in turn increases the absorption coefficient, mainly in the infrared region. At the same time, because of the reduction of the band gap between VB and CB, the minimum energy required for the intrinsic excitation is gradually reduced, so that the absorption coefficient of the visible light region is also significantly improved.

Some specfic electronic data, found by interpreting and analysing the DOS, are listed in Table 2. During the charging process from $Li_4Ti_5O_{12}$ to $Li_7Ti_5O_{12}$, the Fermi level increases from 0.81 eV to 5.7 eV; the energy barrier from VB to donor states decreases from 3.93 eV to 2.39 eV; the donor states appear and expand to 1.28 eV, while the position in the forbidden band continuously moves to the deeper level, leading to the increase of the donor ionization energy from 0.16 eV to 0.67 eV. In the DFT calculation, 24 Li atoms are gradually added into the unit cell, which can provide 24 free electrons. By integrating the area of the donor states in Figure 5, it can be found that these electrons prefer to maintain a high spin state in the d_{xy} orbit. Under equilibrium conditions, more electrons in the donor states means that more electrons are likely to be free ones in the CB. Therefore, the charging process is also a process in which the conductivity of the LTO material is continuously improved.

This mechanism is further supported by considering orbital symmetries. According to the octahedral crystal field effect, the five-fold degenerate $3d$ orbits of Ti split into two groups: t_{2g} (d_{xy}, d_{xz}, d_{yz}) and e_g $(d_{x^2-y^2}, d_{z^2})$. A zoomed in plot highlighting how degeneracies manifest in the PDOS is shown in Figure 6(b), using $Li_{4.125}Ti_5O_{12}$ as an example. As the $2p$ orbits of O decomposed into p_σ and p_π, the molecular-orbital bonding diagram was shown in Figure 6(a), which is in accordance with the electronic structure clearly illustrated in Figure 5: the O p_σ states and the Ti e_g states form the bonding σ states in the low energy region of the valence band (VB), and the anti-bonding σ^* states in the high energy region of the conduction band (CB); the middle region of VB and CB are the weak π bonding between the O p_π states and the Ti t_{2g} states. The valence band maximum (VBM) and the conduction band minimum (CBM) are non-bonding O p_π and Ti t_{2g} states, respectively.

Table 2 Specific electronic data from the DOS

	$Li_4Ti_5O_{12}$	$Li_{4.125}Ti_5O_{12}$	$Li_5Ti_5O_{12}$	$Li_6Ti_5O_{12}$	$Li_7Ti_5O_{12}$
Fermi level (eV)	0.81	4.56	4.91	5.30	5.70
VB to donor states (eV)	3.93	3.12	2.87	2.64	2.39
Width of donor states (eV)	–	0.34	0.76	0.92	1.28
Donor ionization (eV)	–	0.16	0.16	0.44	0.67
Added Li per unit	–	1	8	16	24
Spin up electrons	–	1	5	10	20
Spin down electrons	–	0	3	6	4

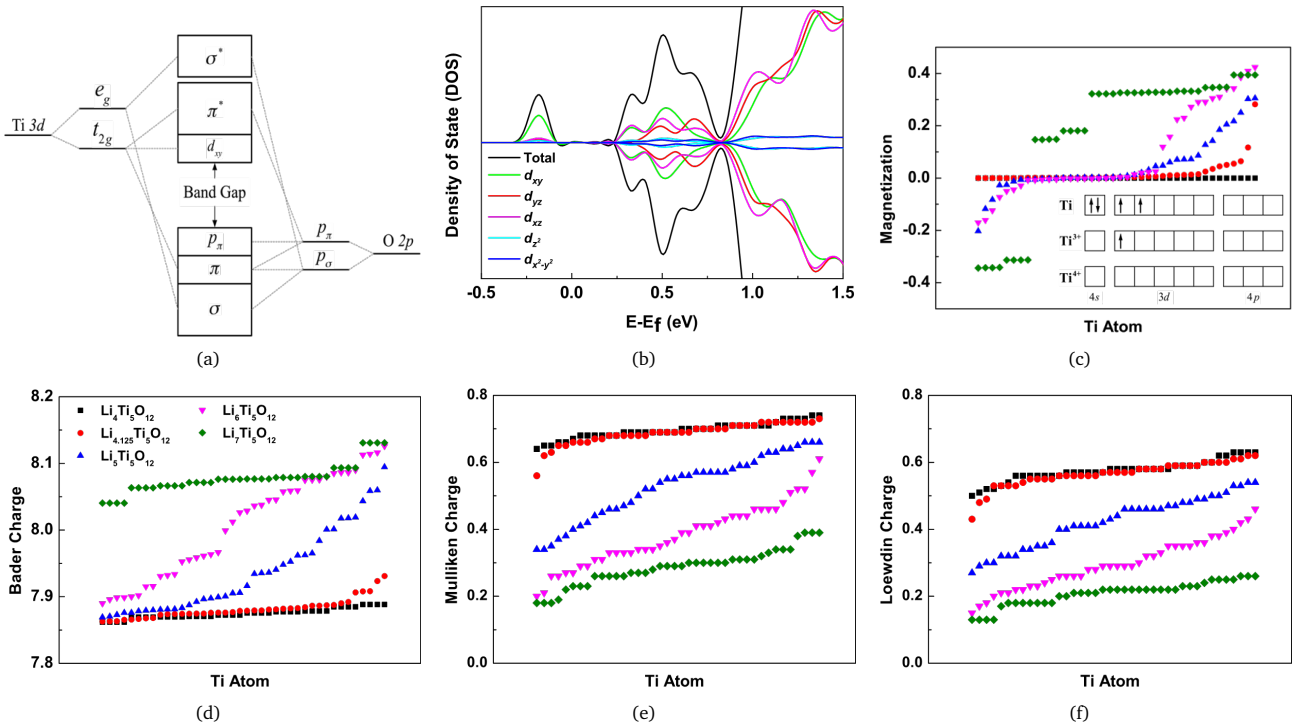

Fig. 6 (a)The molecular-orbital bonding diagram for TiO_6 octahedron; (b)Total and projected densities of states (DOS) of $Li_{4.125}Ti_5O_{12}$ around Fermi level; (c)(d)(e)(f) are Magnetization, Bader charge, Mulliken charge and Loewdin charge of 40 Ti atoms in LTO supercells, showing electron population in different methods. The label of x axis is the number of Ti Atoms. The atom orders are not same in each graph and are sorted in increasing order. Symbols are the same in each graph. The inset of the top-right graph shows the electron configuration of Ti, Ti^{3+}, Ti^{4+}.

3.2 Charge population analysis

Finally, we consider the role played by electrostatics. The $1 \times 1 \times 3$ supercell yields 40 Ti atoms in each structure. The atom order is varied in different graphs, to report results in increasing order of the relevant quantity, for visual clarity. We do not expect information to be lost by this choice. Figure 6(c)-6(f) show the magnetization and effective charges of Ti atoms, which change gradually, rather than concentrating on several discrete values. So all Ti atoms are largely equivalent to each other. There are various theories used to investigate charge distribution in solid systems. To provide a broad overview, free from the quirks of specific analyses, we present effective charge results from Bader, Mulliken and Loewdin population analysis.[25] Agreement between these methods, as seen here, indicates a likely close connection to real charge distribution.

When Li intercalates, Ti is chemically reduced and the valence is lowered, which means the number of extranuclear electrons surrounding Ti is increased from the perspective of wave function. So Bader charge increases (the number of electrons involved in DFT calculation for each Ti atom is 10). From another perspective, more electrons are shared between Ti and O, instead of occupied mainly by O. So Mulliken charge and Loewdin charge decrease. Different charge population methods reflect the same fact. From the electron distribution of Ti^{3+} and Ti^{4+}, it is known that the reduction of Ti^{4+} causes lone pair electrons in d orbit. This can also be confirmed by the Density of State (DOS) calculation (Figure 6(b)), which shows that these electrons are in the d_{xy} orbit.

4 Conclusion

To conclude, this study reports density functional theory calculations of optical properties, density of states (DOS) and charge population analysis of the LTO material during charging/discharging process.

From optical results, the color change process as well as the transmittance in visible and infrared wavelength and its mechanism are theoretically investigated. Importantly, we found that the change in absorption coefficient is not coupled between visi-

ble and infrared wavelengths. The latter is much more sensitive than the former. The energy of transmitted visible light decreases from 17% to 16% when $Li_4Ti_5O_{12}$ is charged to $Li_{4.125}Ti_5O_{12}$, while the energy of transmitted infrared drops sharply from 35% to 21%. This means that, when used as smart windows, temperature control and brightness control can be separated considerably: lowering room temperature without significantly reducing brightness.

Optical performance changes are the external manifestation of changes in electronic structure. From the DOS results, for example, during charging process, the donor states will form, expand and move to deeper levels in the forbidden band. More electrons in the donor states lead to more free electrons in the conduction band under balanced conditions, which explain the rising of conductivity. This conclusion is further supported by electrostatic arguments. Different kinds of charge calculation methods and magnetization results certify that Ti ions are chemically reduced to lower valence during charging and have a high equivalence as charges of different methods change continuously. As positive ion interstitial, higher-valance cation replacement, and negative ion vacancy[26,27] can make similar changes to electronic structure, which are helpful to form donor states, these methods can change the range of variation of the absorption coefficient and finally realize tuning the range of transmittance. This can help LTO achieve a wider range of applications.

To sum up, $Li_4Ti_5O_{12}$ is a promising electrochromic material under visible-to-infrared wavelength with many advantages: large tunable transmittance, wide operating temperature range, excellent cycle stability, low manufacture cost. The results reported here theoretically show that $Li_4Ti_5O_{12}$ can also be used in smart windows, thermal management and infrared camouflage.

References

1 J. Mandal, S. Du, M. Dontigny, K. Zaghib, N. Yu and Y. Yang, *Advanced Functional Materials*, 2018, **28**, 1802180.

2 P.-c. Tsai, W.-D. Hsu and S.-k. Lin, *Journal of the Electrochemical Society*, 2014, **161**, A439–A444.

3 P. Hohenberg and W. Kohn, *Physical Review*, 1964, **136**, B864–B871.

4 W. Kohn and L. J. Sham, *Physical Review*, 1965, **140**, A1133–A1138.

5 G. Kresse and J. Furthmüller, *Computational Materials Science*, 1996, **6**, 15–50.

6 G. Kresse and J. Furthmüller, *Physical Review B*, 1996, **54**, 11169–11186.

7 J. P. Perdew, K. Burke and M. Ernzerhof, *Physical Review Letters*, 1996, **77**, 3865–3868.

8 P. E. Blöchl, *Physical Review B*, 1994, **50**, 17953–17979.

9 Y. Gao, Z. Wang and L. Chen, *Journal of Power Sources*, 2014, **245**, 684–690.

10 Z. Hu and H. Metiu, *The Journal of Physical Chemistry C*, 2011, **115**, 5841–5845.

11 J. Heyd, G. E. Scuseria and M. Ernzerhof, *The Journal of Chemical Physics*, 2003, **118**, 8207–8215.

12 J. Heyd, G. E. Scuseria and M. Ernzerhof, *The Journal of Chemical Physics*, 2006, **124**, 219906.

13 A. V. Krukau, O. A. Vydrov, A. F. Izmaylov and G. E. Scuseria, *The Journal of Chemical Physics*, 2006, **125**, 224106.

14 J. Paier, M. Marsman, K. Hummer, G. Kresse, I. C. Gerber and J. G. Ángyán, *The Journal of Chemical Physics*, 2006, **124**, 154709.

15 B. P. Jelle, *Solar Energy Materials and Solar Cells*, 2013, **116**, 291–323.

16 G. K. Pal and G. K, *Textbook of Practical Physiology*, Orient Longman, 2001.

17 P. A. Buser, M. Imbert, R. H. Kay and M. I. T. Press, *Vision*, MIT Press, 1992.

18 M. Roeder, A. B. Beleke, U. Guntow, J. Buensow, A. Guerfi, U. Posset, H. Lorrmann, K. Zaghib and G. Sextl, *Journal of Power Sources*, 2016, **301**, 35–40.

19 R. J. Mortimer, D. R. Rosseinsky and P. M. S. Monk, *Electrochromic Materials and Devices*, Wiley, 2015.

20 J. Byrnes, *Unexploded Ordnance Detection and Mitigation*, Springer Netherlands, 2008.

21 S. Scharner, W. Weppner and P. Schmid Beurmann, *Journal of the Electrochemical Society*, 1999, **146**, 857–861.

22 K. Sauvet, L. Sauques and A. Rougier, *Solar Energy Materials and Solar Cells*, 2009, **93**, 2045–2049.

23 M. G. Verde, L. Baggetto, N. Balke, G. M. Veith, J. K. Seo, Z. Wang and Y. S. Meng, *ACS Nano*, 2016, **10**, 4312–4321.

24 H. Song, S.-W. Yun, H.-H. Chun, M.-G. Kim, K. Y. Chung, H. S. Kim, B. W. Cho and Y.-T. Kim, *Energy & Environmental Science*, 2012, **5**, 9903–9913.

25 S. Maintz, V. L. Deringer, A. L. Tchougréeff and R. Dronskowski, *Journal of Computational Chemistry*, 2016, **37**, 1030–1035.

26 J. Qiu, C. Lai, E. Gray, S. Li, S. Qiu, E. Strounina, C. Sun, H. Zhao and S. Zhang, *J. Mater. Chem. A*, 2014, **2**, 6353–6358.

27 X. Chen, L. Liu, P. Y. Yu and S. S. Mao, *Science*, 2011, **331**, 746–750.